Intruder configurations of excited states in the neutron-rich isotopes ^{33}P and ^{34}P

R. S. Lubna, Vandana Tripathi, S. L. Tabor, P.-L. Tai, K. Kravvaris, P. C. Bender, A. Volya, M. Bouhelal, C. J. Chiara, M. P. Carpenter, R. V. F. Janssens, T. Lauritsen, E. A. McCutchan, S. Zhu, R. M. Clark, P. Fallon, A. O. Macchiavelli, S. Paschalis, M. Petri, W. Reviol, and D. G. Sarantites

Phys. Rev. C **97**, 044312 — Published 16 April 2018

DOI: 10.1103/PhysRevC.97.044312

Intruder configurations of excited states in the neutron-rich isotopes ^{33}P and ^{34}P

R. S. Lubna, Vandana Tripathi, S. L. Tabor, P.-L. Tai, K. Kravvaris, P. C. Bender,* and A. Volya

Department of Physics, Florida State University, Tallahassee, Florida 32306, USA

M. Bouhelal

Laboratoire de Physique Appliquée et Théorique, Université Labri Tébessa, Tébessa, Algeria

C. J. Chiara†

Argonne National Laboratory, Argonne Illinois 50439, USA and Chemistry and Biochemistry, University of Maryland, College Park, Maryland 20742, USA

M. P. Carpenter, R. V. F. Janssens, T. Lauritsen, E. A. McCutchan, and S. Zhu

Argonne National Laboratory, Argonne Illinois 50439, USA

R. M. Clark, P. Fallon, A. O. Macchiavelli, S. Paschalis, and M. Petri

Lawrence Berkeley National Laboratory, Berkeley, California 94720, USA

W. Reviol and D. G. Sarantites

Washington University, St. Louis, Missouri 63130, USA

(Dated: March 26, 2018)

Abstract

Excited states in the neutron-rich isotopes ^{33}P and ^{34}P were populated by the ^{18}O+^{18}O fusion-evaporation reaction at E_{lab}=24 MeV. The Gammasphere array was used along with the Microball particle detector array to detect γ transitions in coincidence with the charged particles emitted from the compound nucleus ^{36}S. The use of Microball enabled the selection of the proton emission channel. It also helped in determining the exact position and energy of the emitted proton; this was later employed in kinematic Doppler corrections. 16 new transitions and 13 new states were observed in ^{33}P and 21 γ rays and 20 energy levels were observed in ^{34}P for the first time. The nearly 4π geometry of Gammasphere allowed the measurement of γ-ray angular distributions leading to spin assignments for many states. The experimental observations for both isotopes were interpreted with the help of shell-model calculations using the $(0+1)\hbar\omega$ PSDPF interaction. The calculations accounted for both the 0p-0h and 1p-1h states reasonably well and indicated that 2p-2h excitations might dominate the higher-spin configurations in both ^{33}P and ^{34}P.

* Present address: Physics and Applied Physics, University of Massachusetts, Lowell, Massachusetts 01854 USA.

† Present address: US Army Research Laboratory, Adelphi, Maryland 20783, USA.

I. INTRODUCTION

In recent years, the structure of nuclei in the vicinity of the island of inversion has attracted experimental attention in order to untangle the properties of the intruder configuration(s). Phosphorus isotopes, with $Z = 15$ and neutrons occupying the upper *sd* shell, are of considerable interest in this regard as they exhibit an interplay between normal and intruder shell structure at low excitation energies: this can be informative to understand the evolution of shell gaps with a gradual increase in neutron number. Two phosphorus isotopes, odd-mass ^{33}P and even-mass ^{34}P, have been chosen in the present work to contribute to the understanding of the upper *sd* shell nuclei and their intruder configurations.

Numerous studies have previously been conducted on ^{33}P including β-decay of ^{33}Si [1, 2] and particle-transfer reactions like (α, p), (t, p) and $(d,^3\mathrm{He})$ [3–15] to study the excited states. Currie *et al.* [3] observed the first three levels for the first time by means of the $^{30}\mathrm{Si}(\alpha, p)^{33}\mathrm{P}$ reaction. Later, Moss *et al.* [13] assigned spins to those states. Berkowitz *et al.* [8] and Davis *et al.* [12] extended the level scheme up to 6.56 MeV and 10.12 MeV, respectively. The mean lifetimes for the first two excited states were measured first by Currie *et al.* [6] by means of the Doppler Shift Attenuation Method (DSAM) using the (α, p) reaction. Further lifetime analyses had been performed later by Carr *et al.* [10] using (α, p) reaction and also by Poletti *et al.* [16] and Wagner *et al.* [17] using the $(t, p\gamma)$ reaction employing the DSAM method. The fusion-evaporation reactions $^{18}\mathrm{O}(^{18}\mathrm{O},\ p2n\gamma)^{33}\mathrm{P}$ [18] and $^{26}\mathrm{Mg}(^{13}\mathrm{C},\ pn\alpha)^{33}\mathrm{P}$ [19] were conducted recently in order to study higher-energy and higher-spin states.

Most of the previous experimental works on ^{34}P have been summarized in Refs. [20] and [21]. A binary grazing reaction was conducted by Chapman *et al.* [22] to populate the excited states of ^{34}P, where they verified most of the previous transitions and states and compared them with PSDPF shell model calculations. The same data set as the one used in the current work had been used to study ^{34}P in Ref. [21]. The improved analysis with the kinematic Doppler correction of ^{33}P encouraged us also to re-examine ^{34}P and this proved productive. A number of new γ transitions and states has been observed, and spin assignments to some states have been proposed.

This paper is devoted to the experimental investigation and the understanding of excited states of ^{33}P and ^{34}P with the help of shell-model calculations. The use of large γ and particle detector arrays along with the heavy-ion beam offered a powerful tool to study the structure of these two *sd* shell nuclei and the associated intruder configurations. The experimental details relevant for this work are presented in Sec. II. The results and data analyses are discussed in Sec. III. Finally, the experimental results were compared to large-scale shell-model calculations in Sec. IV, while Sec. V presents a summary of the work.

II. EXPERIMENTAL DETAILS AND PROCEDURES

Excited states in ^{33}P and ^{34}P were populated in reactions of ^{18}O ions, accelerated to 24 MeV by the ANL ATLAS accelerator, incident onto an ^{18}O target. A target layer of 260 μg/cm^2 thickness was prepared by the electrolysis of water enriched to 97% in ^{18}O, backed by a 12.7 μm tantalum (Ta) foil.

The deexciting gamma rays were detected by Gammasphere [23], which consisted of 101 Compton-suppressed HPGe detectors arranged in 16 rings, each corresponding to a constant polar angle θ with respect to the beam axis. In the Gammasphere cavity, the nearly 4π detector Microball [24], an array of 95 CsI(Tl) scintillators, was installed to detect and identify protons and other evaporated light charged particles.

A ^{152}Eu source has been used in order to perform the energy calibration, which was verified later by using peaks with higher energies from room background and induced activities. The calibration remained very linear up to 4122.5 keV with deviations of less than 0.2 keV. Events were selected offline, in which exactly one proton was detected. The correlated γ rays were sorted into $\gamma - \gamma$ coincidence matrices of various types (see below). As the neutrons were not detected, new transitions in ^{33}P and ^{34}P were assigned by their coincidence relationships with known γ rays. The energies and approximate angles with respect to the beam axis of the recoiling evaporation-residue nuclei were determined event-by-event by a kinematic reconstruction procedure using the measured proton energies and angles [25]. This information was subsequently used to improve the Doppler-shift corrections of

the γ-ray energies, where applicable. This procedure significantly improved the energy resolution of the γ spectra even though the effect on the recoil angle by the evaporated neutron(s) could not be included in the reconstruction. Figure 1 illustrates how much the energy resolution was improved, and, hence, the importance of the reanalysis of ^{34}P after the kinematic reconstruction.

Another issue in the analysis was introduced by the thick target backing. Decays from the long-lived states occurred after the residual nucleus had come to rest (no Doppler shift), while transitions from shorter-lived states were nearly fully shifted. To make full use of the data, three types of proton-gated $\gamma - \gamma$ matrices were produced from the data without any or only one axis or both axes Doppler corrected.

The nearly 4π geometry of Gammasphere provided the ability to measure angular distributions for many of the transitions seen in the present work. The angular distribution analysis was performed with the data sorted into asymmetric coincidence matrices, which contained the γ energies recorded in a set of detectors in an individual ring along one axis, and the energies deposited in all other detectors along the other axis. The γ intensities were normalized based on a ^{152}Eu source. In the analysis, the magnetic sub-state distribution of the initial state was treated as a Gaussian distribution with a width σ =1.4. This parameter value was kept constant for all the states, following the argument presented by Taras *et al.* [26]. Theoretical angular distributions were calculated using the code AD [27] as a function of spin hypotheses and mixing ratios δ using the formalism of Rose and Brink [28]. The goodness of fit χ^2 was measured as a function of possible mixing ratios ranging from minus to plus infinity for different spin hypotheses. All the fits from the angular distribution whose goodness of fit χ^2 were below the 0.1% confidence limit were considered to be acceptable, except for E2 decay hypotheses where only $\chi^2 < 0.1\%$ for $\delta = 0$ was considered acceptable.

III. RESULTS AND ANALYSES

Prior to this work, an experiment was conducted by Chakrabarti *et al.* [18] using the same reaction to study both ^{33}P and ^{34}P. In that work, 5 clover detectors with no particle detector

were used. As stated above, the use of Microball in the current measurement enabled us to perform a kinematic Doppler correction, and achieved better energy resolution of the fast transitions. Gammasphere being an array of large number of detectors offered better event statistics as well. A number of new lines and states were thus added in both isotopes. The level schemes were updated and extended, and spin assignments to some states are proposed.

A. ^{33}P

Figure 2 presents the level scheme of ^{33}P constructed in the current work. Most of the previously reported transitions and states have been confirmed, and 16 new γ transitions and 13 new states have been observed: these are all marked in red (gray). In a recently published paper [19], ^{33}P was studied with the fusion-evaporation reaction ^{26}Mg(^{13}C, $np\alpha$)^{33}P, where the level scheme was extended up to 10106-keV excitation energy. In the present work, a number of new states which decay to the 1848- and 2539-keV levels were observed for the first time, in addition to the levels reported in [19]. The level energies along with the corresponding transitions, spins, parities and relative intensities are summarized in Table I.

Some examples of the newly observed γ transitions are given in Figure 3. The spectrum in panel (a) was gated on the 1848-keV γ line from the non-Doppler corrected axis of the $\gamma-\gamma$ matrix projecting onto the Doppler corrected one. The spectra in parts (b) through (d) were gated by some of the individual peaks in panel (a) and demonstrate the clear presence of the 1848-keV peak in spectra with no Doppler correction.

Two new γ transitions at 4022- and 4227-keV were observed in the decays of previously reported states at 5453 ($9/2^-$) and 4227 ($7/2^-$) keV, respectively. According to the assigned spins of the parent and the daughter states, both the transitions are of E3 character which is less common. The coincidence spectra confirming the placement of the 4227 transition are presented in Figure 4.

Two new states at 6424- and 6555-keV were established by observing the transitions at 2796- and 2927-keV, decaying to the 3628 keV level. It should be pointed out that the 2796-keV transition is a doublet with the previously known 2795-keV line which feeds the

1432-keV state. This was confirmed by the observation of narrow lines at 2795 keV in the 1226-, 1412- and 1432-keV coincidence gates and broader lines at a similar energy in the 1780-, 1848- and 2196-keV ones.

A state at 6807 keV was established by Fu *et* al. [19] through the observation of two γ transitions at 1168 and 2581 keV. These transitions are confirmed in the present work, although with slightly higher energies of 1171 and 2586 keV, suggesting an energy of 6810 keV for the parent state. Both of the transitions involved are fully Doppler shifted, and were observed in different gates of the Doppler corrected matrix.

The coincidence spectrum obtained by gating on the well-established 2539-keV transition while projecting on the Doppler-corrected axis has confirmed the previously observed γ rays at 1510, 2515 and 2653 keV and revealed new lines at energies of 2877, 3271, 3964 and 4087 keV, as shown in Figure 5. These new transitions give rise to the new states at 5416, 5810, 6502 and 6625 keV, respectively. A state at 5410 keV with two decay branches to the 1848- and 2539-keV levels was reported [15] based on a $(t, p\gamma)$ measurement using NaI scintillators. Almost simultaneously, the same group published another $(t, p\gamma)$ measurement [16] using a small volume Ge(Li) detector which provided higher-energy resolution, but lower efficiency than the NaI scintillator. Only the stronger decay branch was reported in that paper with an energy of 3557.4 (28) keV. In the present Gammasphere experiment, both decays are observed, but their energies suggest two states at 5406 and 5416 keV. A single state solution can not be completely ruled out, but is less likely.

An interesting pattern appears in the widths of γ rays from the states above 5 MeV. The lines from the 5453 and 5639 keV levels are narrow; e.g., consistent with the reported [11] mean lifetimes of 24 and 9.7 ps. However most of the γ rays from the levels above this energy are broad and clearly visible only after implementation of the kinematic Doppler correction. But the transitions from the highest two states observed at 9078 and 10106 keV are narrow, exhibiting no Doppler shift. This could signify a different configuration for the highest energy state at 10106 keV, whose slow decay results in a narrow gamma peak from the 9078 keV level.

Some examples of angular distributions and fits are presented in Figure 6. The χ^2 fit for the 3559-keV line deexciting the 5406-keV state, to the $5/2^+$, 1848-keV level is consistent with $\Delta J = 1$ or 0, but not $\Delta J = 2$ decay. The tendency of fusion-evaporation reaction to populate higher-lying high-spin states suggests spin of 7/2 for the state. Positive parity is likely since they decay to a positive-parity level, rather than to the 4227-keV, $7/2^-$ state.

The 6936-keV state was first reported by Chakrabarti *et al.* [18] through the observation of a 1298-keV γ ray, which they reported to be of quadrupole character, and assigned spin 15/2 to this level. However, Fu *et al.* [19] have shown the transition to be of dipole character by employing the $\gamma\gamma$ angular correlation method, hence, suggesting spin 9/2 or 13/2. In the current study, the angular distribution of the 1298-keV line clearly ruled out a $\Delta J = 2$ transition (Figure 6 (c),(d)) favoring a $\Delta J = 1$ multipolarity instead. From the χ^2 fit, it can be seen that both spins 9/2 and 13/2 are equally acceptable. The tendency of fusion-evaporation reactions to favor higher-spin states makes a 13/2 assignment more likely.

B. ^{34}P

Results for ^{34}P from an earlier analysis of the same data set were published in Ref. [21]. In the present analysis, the Doppler correction has been improved by kinematic reconstruction, as displayed in Figure 1. As a result, 20 additional excited states have been discovered. The level scheme, presented in Figure 7, displays all the known states along with the decay paths of the newly discovered ones which are marked in red (gray). It is worth mentioning that all the new transitions were observed while gating around a narrow peak and projecting onto the Doppler corrected axis of the matrix, implying that the new states are short lived. The level energies of the new states, along with the corresponding transitions, spins, parities and relative intensities are summarized in Table II.

Most of the new states were observed to decay to the lowest 3^-, 4^- and 5^- levels, although three decays proceed directly to the 2^+ level at 429 keV. Many of these transitions can be seen in the portion of the γ spectrum in coincidence with the 429-keV line of Figure 1(b). The coincidence relations have been confirmed by gating on the new γ rays, examples

of which are presented in Figures 8(a) and 8(b). In the earlier analysis [21], a transition at 2960 keV was reported and placed on the top of the 2321-keV state. However, with the improved Doppler-corrected spectra, it is clear that the transition energy is 2942 keV, and decaying into the 3352-keV state instead (Figure 9). Also with the better resolution after kinematic Doppler-correction, we could not confirm 2828 keV transition observed in Ref. [21], and hence decided not to include this transition and the corresponding level at 6180 keV in our updated level scheme. The level at 4447 keV was updated as 4455 keV with the improved resolution.

χ^2 graphs of the measured angular distributions for transitions at 1357, 3571, 2134 keV are compared as functions of the mixing ratio δ for several possible spin sequences in Figure 10. The corresponding angular distributions have also been presented. The χ^2 fits rule out $\Delta J = 2$ transitions for the 1357 and 3571 keV lines, which is also reflected in the corresponding angular distributions. This, along with the fact that fusion evaporation reactions favor higher spin states, suggests that $J = 6$ is most likely for the 4710 and 6923 keV states. The angular distribution of the 2134 keV line is consistent with the previous suggestion of $J = (4^-)$, but does not rule out $J = 3$ by itself.

IV. SHELL-MODEL CALCULATIONS AND DISCUSSION

The experimental results have been compared to theoretical predictions generated by shell-model calculations using the code COSMO [29]. The PSDPF interaction of Ref. [30], developed in the *p-sd-pf* model space outside a closed ^{4}He core, has been used to interpret the available data. The interaction enabled us to calculate not only the $0\hbar\omega$ excitations, but also the $1\hbar\omega$ ones which include both the lower $0p$ and upper fp shells. A key question is whether enough states with quantum number consistent with the energy and decay patterns are predicted to account for the newly observed states as well as the previously reported ones. Tables III and IV answer this question in the affirmative. There is at least one good theoretical candidate for each experimental state. We emphasize that this correspondence is not always unique and should not be considered firm.

Configurations associated with the lower-energy, positive-parity states of ^{33}P involve the valence nucleons confined to the *sd* shell. The positive-parity states up to 4048 keV are in satisfactory agreement with the calculated ones (with ΔE $\approx$ 150 keV) generated with no particle-hole excitation; i.e., they correspond to $0\hbar\omega$ excitations. Even beyond this energy, the differences between the experiment and theory are less than 300 keV. The newly observed state at 5729 keV matches best with a calculated one at 5912 keV, according to the decay pattern and the suggested spin. Also, the new levels at 6424, 6502, 6555 and 6625 keV can be compared to the calculated ones at 6510, 6364, 6554 and 6536 keV, respectively. Since no angular distribution measurement was possible for the reported states, only excitation energies were considered in order to match data with their theoretical counter parts. Negative-parity states in ^{33}P can be obtained by promoting one particle from the orbital $0p$ to the *sd* shell or from the *sd* to the fp shell, giving rise to 1p-1h intruder states. The first negative-parity level at 4227 keV was originally reported by Davies *et al.* [9], where the state was found to be populated by a $\ell = 3$ transfer by measuring the proton angular distribution. In that work, spin-parity values of $7/2^-$ were suggested, representing a 1p-1h excitation, although no theoretical counter-part could be calculated at that time. Later, the spin of the state was confirmed to be 7/2 by Harris *et al.* [7] employing a proton-gamma angular correlation. Until Fu *et al.* [19] calculated this level with the PSDPF interaction, no satisfactory description of this state could be achieved. In a naive picture, it can be predicted that this level is formed by the promotion of an unpaired proton from the $1s_{1/2}$ orbital to the $0f_{7/2}$ orbital, giving rise to the $7/2^-$ spin and parity. But the calculations presented here suggest that this state does not correspond to a pure proton excitation; rather, it has a mixed configuration with 32% $\nu f_{7/2}$ and 46% $\pi f_{7/2}$ occupancy. The observed yrast $9/2^-$ and $11/2^-$ states at 5453 and 5639 keV, on the other hand, are dominated by a one neutron excitation, according to the calculations. The experimental level at 6936 keV can be compared to the calculated 7222-keV state with a configuration dominated by a one-neutron excitation to the $0f_{7/2}$ orbital with some rearrangements of the population of nucleons inside the *sd* shell. The state at 9078 keV was observed by Fu *et al.* [19] and their $\gamma\gamma$ angular correlation analysis restricted the possible spin to (7/2, 11/2, 15/2). A $15/2^-$, 9094-keV state was obtained in the calculations and is likely to be the theoretical counter-part of the observed one. The calculated levels corresponding to the observed negative-parity states, except the first $7/2^-$ state, appear to be mainly associated with a neutron excitation to the

fp shell, predominantly to the $0f_{7/2}$ orbital.

The non-yrast states at 5406, 5416, 5810, 5926, 5991, 7998 and 8086 keV in ^{33}P observed in the present work did not appear to have theoretical counter-parts in calculations with nucleons confined to the *sd* shell; i.e., limited to $0\hbar\omega$ excitations. Shell-model calculations with the PSDPF interaction could predict these states as $1\hbar\omega$ excitation, where the configurations are dominated by one-neutron excitations from the *sd* to the fp shell.

Figure 11 illustrates the observed yrast negative-parity states and the corresponding PSDPF levels along with the fp shell occupancies for ^{33}P and nearby odd-mass phosphorus isotopes. It can be seen that the first negative-parity states of all the isotopes are $7/2^-$ levels as expected, and are generated by a mixed proton-neutron excitation from the sd shell. For ^{31}P, an unpaired proton and a pair of neutrons occupy the $0s_{1/2}$ orbital in the ground-state configuration. So, it is expected that the first negative-parity 7/2 state of ^{31}P will correspond predominantly to a proton excitation across the *sd-pf* shell gap. However, shell-model calculations with the PSDPF interaction indicate that the state has almost equal contributions from protons and neutrons. The energy of the level is overestimated by more than 300 keV. This corresponds to the cost of breaking a pair of neutrons and having a significant occupation of the $0f_{7/2}$ orbital. All other yrast, negative-parity states in ^{31}P are also described by equal contributions of proton and neutron excitations to the fp shell. Unlike ^{31}P, the yrast negative-parity states in ^{33}P and ^{35}P are dominated by one-neutron excitations to the fp shell, except the first $7/2^-$ level.

The highest observed state at 10106 keV was first reported by Fu *et al.* [19] and is confirmed in the current work. The angular correlation measurement in the Ref. [19] restricted possible spin values to (13/2, 17/2). The shell-model calculations predict two nearby levels at 10554 ($13/2^+$) and 11239 ($17/2^-$) keV. A 13/2 spin was considered more probable in Ref. [19]. However, the possibility of spin 17/2 cannot be excluded, as an yrast or near-yrast decay sequence should be anticipated when a fusion-evaporation reaction is used, as in the case here, although the first calculated $17/2^-$ state is predicted to lie more than 1 MeV higher. The nearest 0p-0h, $17/2^+$ state computed with the PSDPF interaction is at 14460 keV. This overestimation might be an indication that a $2\hbar\omega$ excitation towards the fp shell

needs to be considered. Following the arguments above about the 6936-and 9078-keV states being of 1p-1h character, the 10106-keV level may well correspond to a 2p-2h configuration which decays via the 1p-1h excitations. This would be consistent with the electromagnetic operator being a one body operator. Also, the narrow width of γ transitions emitted from the 10106-keV level indicate a relatively long lifetime for this state and this supports the argument. A similar feature was observed in ^{31}P [31], where the experimental $15/2^+$ and $17/2^+$ states at energies 10520 and 11297 keV, respectively, could not be explained by $0\hbar\omega$ excitations within calculations with the USD interaction. The use of the SDPF-M interaction [32] described the 0p-0h positive-parity states well up to the yrast $13/2^+$ state. This interaction calculated the $15/2^+$ and $17/2^+$ levels as resulting from the promotion of one proton and one neutron from the *sd* to the *fp* shell, and the computed energies of 10230 and 11720 keV, respectively, were close to the observed states. Also, the configuration of the states supported the decay pattern observed in the experiment. With a very similar yrast sequence in ^{33}P, and considering the features discussed above, the level at 10106 keV is likely to be associated with a 2p-2h intruder state in ^{33}P. This is, however, beyond the scope of the calculations presented in this paper.

The agreement between theory and experiment in ^{33}P was the motivation to use the same approach with the PSDPF interaction to describe ^{34}P as well. Again, the spectrum for this isotope is well described with this interaction. In fact, all the experimentally observed states in the present work have a likely PSDPF counter-part (see table IV), except the state at 6237 keV, which will be discussed later. As in other such nuclei, the positive-parity states are characterized as $0\hbar\omega$ excitations and the negative-parity levels correspond to $1\hbar\omega$ ones, with the PSDPF interaction being limited to only one-particle excitations either from the $0p$ to the *sd* shell or from the *sd* shell to the *pf* one above it. Though the PSDPF interaction results in a wide range of 0p-0h levels, only a few positive-parity state were observed in earlier work, and those are described satisfactorily. Three new levels were observed here which decay to the first excited state at 429 keV (2^+). Considering their decay pattern, those are assumed to have positive parity. There are likely positive-parity theoretical counter-parts with energy differences of less than 250 keV for them. All other new states decay to the negative-parity levels. Their decay patterns and the angular distribution measured from some transitions suggest that those states are of negative parity and, hence, arise from one-

particle excitations from the sd to the fp shell. All the theoretical counter-parts of these states have configurations dominated by neutron excitations, mainly to the $0f_{7/2}$ orbital.

Like for the odd-mass phosphorus nuclei, Figure 12 depicts the comparison between the experimental and theoretical yrast negative-parity states along with the fp shell occupancies of the even-mass ^{32}P and ^{34}P isotopes. For both nuclei, all the states calculated with the PSDPF interaction, plotted in the picture are mainly associated with a neutron excitation. This is expected as ^{32}P and ^{34}P both have one unpaired proton occupying the $s_{1/2}$ orbital and one unpaired neutron residing in the $d_{3/2}$ one. Being energetically efficient, the excitations of the unpaired neutron across the fp shell are favored and give rise to the negative-parity intruder states.

The state observed at 6237 keV was first reported by Ollier *et al.* [33], where they proposed a stretched 7^+ $\pi(\mathrm{f}_{7/2})$ $\nu(\mathrm{f}_{7/2})$ configuration. Later, Bender *et al.* [21] verified the energy and the spin of the level using the present data set, and those authors agreed with the previous argument that the level likely corresponds to a 2p-2h intruder, 7^+ excitation. Also, the first 7^+ state in the PSDPF calculation is at 10712 keV, and is a 0p-0h state; i.e., there is no good candidate for the observed state in the present theoretical spectrum, in line with the suggestion of a 2p-2h configuration.

V. SUMMARY

A detailed investigation of the structure of ^{33}P has been performed using the Gammasphere array combined with the Microball particle detector array. The level scheme of ^{33}P has been extended with the identification of 16 new transitions and 13 new states. The improved Doppler correction achieved by employing kinematic reconstruction of emitted charged particles also encouraged us to reanalyze ^{34}P. This resulted in the addition of 21 new transitions and 20 new levels to the level scheme. Spin assignments for some of the states in both the isotopes have been proposed based on the measured angular distributions of the emitted transitions. Large-scale shell-model calculations using the $(0+1)\hbar\omega$ PSDPF interaction have been performed in order to interpret the results. In both isotopes, these

calculations provide good candidates for the observed positive- and negative-parity states. The decay pattern and the likely long lifetime of a level at 10106 keV is understood as a likely $2\hbar\omega$ configuration in ^{33}P. A similar feature had been previously proposed in ^{34}P for a level at 6237 keV. In the future $2\hbar\omega$ shell-model calculations would be desirable to better understand the intruder configurations for *sd*-shell nuclei.

ACKNOWLEDGMENTS

This work was supported by U.S. National Science Foundation under grant NSF 140-1574 and the U.S. Department of Energy Office of Science, Office of Nuclear Physics under grants No. DE-SC0009883 (FSU), DE-AC02-05CH-11231 (LBNL), DE-AC02-06CH-1137 (ANL), DE-FG02-88ER-40406 (W.U.), and DE-FG02-94ER-40834 (UMD). This research used resources of ANL's ATLAS facility, which is a DOE Office of Science User facility.

[1] D. R. Goosman and D. E. Alburger, Phys. Rev. C **5**, 1252 (1972).

[2] D. R. Goosman, C. N. Davids, and D. E. Alburger, Phys. Rev. C **8**, 1324 (1973).

[3] W. M. Currie and J. E. Evans, Phys. Lett. B **24**, 399 (1967).

[4] R. C. Bearse, D. H. Youngblood, and J. L. Yntema, Phys. Rev. **167**, 1043 (1968).

[5] G. Hardie, R. E. Holland, L. Meyer-Schützmeister, F. T. Kuchnir, and H. Ohnuma, Nucl. Phys. A **134**, 673 (1969).

[6] W. M. Currie, L. G. Earwaker, J. Martin, and A. K. Sen Gupta , Phys. Lett. B **28**, 480 (1969).

[7] W. R. Harris, K. Nagatani, and J. W. Olness, Phys. Rev. C **2**, 1412 (1970).

[8] E. H. Berkowitz, Nucl. Phys. A **140**, 173 (1970).

[9] W. G. Davies, J. C. Hardy, and W. Darcey, Nucl. Phys. A **128**, 465 (1969).

[10] P. E. Carr, D. C. Bailey, J. L. Durell, L. L. Green, A. N. James, J. F. Sharpey-Schafer, and D. A. Viggars, J. Phys. A **6**, 685 (1973).

[11] M. R. Nixon, G. D. Jones, P. R. G. Lornie, A. Nagel, P. J. Nolan, H. G. Price, and P. J. Twin, Nucl. Phys. **1**, 430 (1975).

[12] N. J. Davis and J. M. Nelson, Nucl. Phys. **13**, 375 (1987).

[13] C. E. Moss, R. V. Poore, N. R. Roberson, and D. R. Tilley, Phys. Rev. **174**, 1333 (1968).

[14] S. Khan, G. Mairle, K. T. Knöpfle, Th. Kihm, Liu-Ken Pao, P. Grabmayr, G. J. Wagner, and L. Friedrich, Nucl. Phys. A **122**, 150 (1988).

[15] A. R. Poletti, T. T. Bardin, R. E. McDonald, and J. G. Pronko, Phys. Rev. C **7**, 1479 (1973).

[16] A. R. Poletti, T. T. Bardin, J. G. Pronko, and R. E. McDonald, Phys. Rev. C **7**, 1433 (1973).

[17] P. Wagner, J. P. Coffin, M. A. Ali, D. E. Alburger, and A. Gallmann, Phys. Rev. C **7**, 2418 (1973).

[18] R. Chakrabarti, S. Mukhopadhyay, Krishichayan, A. Chakraborty, A. Ghosh, S. Ray, S. S. Ghugre, A. K. Sinha, L. Chaturvedi, A. Y. Deo, I. Mazumdar, P. K. Joshi, R. Palit, Z. Naik, S. Kumar, N. Madhavan, R. P. Singh, S. Muralithar, B. K. Yogi, and U. Garg, Phys. Rev. C **80**, 034326 (2009).

[19] B. Fu, M. Seidlitz, A. Blazhev, M. Bouhelal, F. Haas, P. Reiter, K. Arnswald, B. Birkenbach, C. Fransen, G. Friessner, A. Henning, H. Hess, R. Hirsch, L. Lewandowski, D. Schneiders, B. Siebeck, T. Steinbach, T. Thomas, A. Vogt, A. Wendt, K. Wolf, and K. O. Zell, Phys. Rev. C **94**, 034318 (2016).

[20] P. C. Bender, C. R. Hoffman, M. Wiedeking, J. M. Allmond, L. A. Bernstein, J. T. Burke, D. L. Bleuel, R. M. Clark, P. Fallon, B. L. Goldblum, T. A. Hinners, H. B. Jeppesen, Sangjin Lee, I.-Y. Lee, S. R. Lesher, A. O. Macchiavelli, M. A. McMahan, D. Morris, M. Perry, L. Phair, N. D. Scielzo, S. L. Tabor, Vandana Tripathi, and A. Volya, Phys. Rev C **80**, 014302 (2009).

[21] P. C. Bender, S. L. Tabor, Vandana Tripathi, C. R. Hoffman, L. Hamilton, A. Volya, R. M. Clark, P. Fallon, A. O. Macchiavelli, S. Paschalis, M. Petri, M. P. Carpenter, R. V. F. Janssens, T. Lauritsen, E. A. McCutchan, D. Seweryniak, S. Zhu, C. J. Chiara, X. Chen, W. Reviol, D. G. Sarantites, and Y. Toh, Phys. Rev. C **85**, 044305 (2012).

[22] R. Chapman, A. Hodsdon, M. Bouhelal, F. Haas, X. Liang, F. Azaiez, Z. M. Wang, B. R. Behera, M. Burns, E. Caurier, L. Corradi, D. Curien, A. N. Deacon, Zs. Dombrádi, E. Farnea, E. Fioretto, A. Gadea, F. Ibrahim, A. Jungclaus, K. Keyes, V. Kumar, S. Lunardi, N. Mărginean, G. Montagnoli, D. R. Napoli, F. Nowacki, J. Ollier, D. O'Donnel, A. Papenberg, G. Pollarolo, M.-D. Salsac, F. Scarlassara, J. F. Smith, K. M. Spohr, M. Stanoiu, A. M. Stefanini, S. Szilner, M. Trotta, and D. Verney, Phys. Rev. C **92**, 044308 (2015).

[23] GAMMASPHERE, `https://www.phy.anl.gov/gammasphere/`.

[24] D. G. Sarantites, P.-F. Hua, M. Devlin, L. G. Sobotka, J. Elson, J. T. Hood, D. R. LaFosse, J. E. Sarantites, and M. R. Maier, Nuclear Instruments and Methods in Physics Research Section A: Accelerators, Spectrometers, Detectors and Associated Equipment **381**, 418 (1996).

[25] P.-L. Tai, Ph.D dissertation (unpublished) (2016).

[26] P. Taras and B. Haas, Nuclear Instruments and Methods in Physics Research Section A: Accelerators, Spectrometers, Detectors and Associated Equipment **123**, 73 (1975).

[27] E. F. Moore, Ph.D dissertation (unpublished) (1988).

[28] H. J. Rose and D. M. Brink, Rev. Mod. Phys. **39**, 306 (1967).

[29] A. Volya, `http://www.volya.net/`.

[30] M. Bouhelal, S. Haas, E. Caurier, F. Nowacki, and A. Bouldjedri, Nucl. Phys. A **864**, 113 (2011).

[31] M. Ionescu-Bujor, A. Iordachescu, D. R. Napoli, S. M. Lenzi, N. Mărginean, T. Otsuka, Y. Utsuno, R. V. Ribas, M. Axiotis, D. Bazzacco, A. M. Bezzeti-Sona, P. G. Bezzeti, F. Brandolini, D. Bucurescu, M. A. Cardona, G. de Angelis, M. De Poli, F. Della Vedova, E. Farnea, A. Gadea, D. Hojman, C. A. Kalfas, T. Kröll, S. Lunardi, T. Martínez, P. Mason, P. Pavan, B. Quintana, C. Rossi Alvarez, C. A. Ur, R. Vlastou, and S. Zilio, Phys. Rev. C **73**, 024310 (2006).

[32] Y. Utsuno, T. Otsuka, T. Glasmacher, T. Mizusaki, and M. Honma, Phys. Rev. C. **70**, 044307 (2004).

[33] J. Ollier, R. Chapman, X. Liang, M. Labiche, K.-M. Spohr, M. Davison, G. de Angelis, M. Axiotis, T. Kröll, D. R. Napoli, T. Martinez, D. Bazzacco, E. Farnea, S. Lunardi, A. G. Smith, and F. Haas, Phys. Rev. C **71**, 034316 (2005).

TABLE I: Observed excitation energies and spins together with the associated transitions and their relative intensities for levels in ^{33}P. The spins which could not be measured in the current analysis are not listed in this table. The new states and transitions are shown in boldface (normal text).

E_x (keV)	J^π	E_γ (keV)	I_γ
1431.8 (4)	$3/2^+$	1431.8 (4)	64.2 (1)

TABLE I – **Continued from previous page**

E_x (keV)	J^π	E_γ (keV)	I_γ
1847.8 (4)	$5/2^+$	1847.8 (4)	100.0 (1)
		416.0 (4)	13.0 (1)
2538.8 (11)		2539.2 (20)	5.2 (1)
		1106.4 (15)	2.1 (1)
		690.4 (10)	1.6 (2)
3490.7 (11)	$5/2^+$	3490.4 (14)	0.3 (2)
		2058.7 (12)	1.2 (2)
		1643.2 (10)	2.3 (3)
3627.9 (14)	$7/2^+$	2196.3 (15)	13.5 (4)
		1779.9 (13)	7.3 (7)
4048.3 (21)	$5/2^+$	2616.2 (21)	7.1 (1)
		1509.9 (19)	0.4 (1)
4226.6 (10)	$7/2^-$	**4227.0 (15)**	**0.2 (1)**
		2794.6 (13)	0.4 (1)
		2378.6 (9)	47.3 (4)
		735.9 (5)	4.4 (3)
4856.3 (25)		3008.5 (25)	2.4 (3)
5054.5 (23)	$5/2^+$	3623.8 (26)	1.3 (2)
		3206.5 (25)	2.5 (2)
		2514.7 (20)	0.3 (1)
5189.7 (23)		3757.8 (25)	1.4 (3)
		3340.9 (28)	0.8 (3)
		2652.8 (20)	0.3 (1)
5406.4 (25)	**(7/2)**	**3558.6 (25)**	**4.1 (5)**
5415.8 (28)		**2877.0 (26)**	**0.4 (1)**
5452.8 (12)	$9/2^-$	**4021.6 (17)**	**0.2 (1)**
		3605.1 (16)	0.4 (1)

TABLE I – **Continued from previous page**

E_x (keV)	J^π	E_γ (keV)	I_γ
		1825.4 (8)	2.4 (1)
		1226.4 (6)	27.5 (3)
5503.1 (21)		3655.3 (25)	1.3 (3)
		1276.7 (18)	1.0 (2)
5638.8 (12)	$11/2^-$	1412.2 (7)	20.7 (3)
		185.9 (8)	15.9 (2)
5728.6 (25)	**(7/2)**	**3880.8 (25)**	**1.4 (3)**
5810.1 (28)		**3271.3 (26)**	**0.10 (5)**
5925.6 (26)	**(7/2)**	**4077.8 (26)**	**3.0 (2)**
5991.4 (30)		**4143.6 (30)**	**0.7 (3)**
6324.9 (30)		**4477.1 (30)**	**0.8 (3)**
6423.7 (27)		**2795.8 (23)**	**2.3 (5)**
6502.4 (30)		**3963.6 (28)**	**0.10 (5)**
6555.3 (28)		**2927.4 (24)**	**1.2 (3)**
6625.3 (30)		**4086.5 (28)**	**0.2 (2)**
6809.9 (27)	(9/2)	2586.2 (30)	0.8 (3)
		1170.9 (24)	1.0 (4)
6936.4 (22)	(13/2)	1297.6 (18)	4.6 (2)
6987.4 (21)		2760.8 (19)	0.4 (2)
7998.0 (23)		**2359.2 (20)**	**0.4 (2)**
8086.3 (25)	**(13/2)**	**2632.0 (24)**	**0.6 (3)**
		2448.0 (22)	**1.0 (3)**
9078.3 (27)		2142.0 (17)	0.2 (1)
		2090.7 (15)	0.10 (5)
10106.4 (29)		3170.3 (19)	0.2 (1)
		1027.6 (13)	0.7 (3)

TABLE II: Observed excitation energies and spins together with the associated transitions and their relative intensities for levels in ^{34}P. The spins which could not be measured in the current analysis are not listed in this table. The new states and transitions are shown in boldface (normal text). States above 3352 keV that were observed in Ref [21] and verified in the present work are not shown in the table.

E_x (keV)	J^π	E_γ (keV)	I_γ
429.1 (4)	2^+	429.1 (4)	100.0 (1)
2304.9 (6)	4^-	1875.8 (6)	77.7 (1)
2320.6 (7)	3^-	1891.5 (7)	12.2 (1)
3352.4 (10)	5^-	1047.3 (8)	20.2 (1)
		1031.6 (9)	0.64 (2)
3806.3 (26)		**3377.2 (26)**	**1.2 (2)**
4424.0 (27)		**3994.9 (27)**	**4.7 (2)**
4570.7 (21)		**2250.1 (20)**	**1.0 (3)**
4613.1 (22)		**2292.5 (21)**	**0.8 (2)**
4710.0 (21)	**(6)**	**2405.5 (20)**	**6.3 (3)**
		1356.9 (23)	**2.1 (7)**
4729.3 (30)		**4300.2 (30)**	**0.5 (2)**
5344.2 (29)		**3039.3 (28)**	**2.6 (6)**
5594.1 (26)		**3289.2 (25)**	**1.1 (5)**
5788.3 (29)		**3483.4 (28)**	**1.1 (8)**
5975.3 (30)		**3670.4 (29)**	**1.5 (5)**
6118.2 (31)		**3813.3 (30)**	**0.8 (6)**
6174.2 (29)		**3869.3 (28)**	**1.3 (3)**
6294.6 (24)		**2942.2 (21)**	**4.0 (8)**
6316.5 (31)		**4011.6 (30)**	**0.60 (5)**
6444.7 (31)		**4139.8 (30)**	**1.3 (8)**

TABLE II – **Continued from previous page**

E_x (keV)	J^π	E_γ (keV)	I_γ
6923.0 (28)	**(6)**	**3570.6 (26)**	**0.60 (9)**
6990.9 (30)		**3638.5 (28)**	**0.8 (3)**
7065.6 (27)		**3713.2 (25)**	**0.20 (5)**
7256.1 (27)		**3903.7 (25)**	**0.30 (5)**
7590.4 (33)		**4238.0 (31)**	**1.0 (4)**

TABLE III: Possible correspondences between states calculated in the shell model for ^{33}P using the PSDPF interaction and the observed states. The calculation comprises both 0p-0h (positive-parity) and 1p-1h (negative-parity) states. The newly observed experimental states are shown in boldface (normal text). The last column expresses the energy difference between experimental and estimated states (ΔE).

J_i^π	PSDPF (keV)	Exp (keV)	ΔE (keV)
$3/2_1^+$	1441	1432	-9
$5/2_1^+$	1905	1848	-57
$3/2_2^+$	2679	2539	-140
$5/2_2^+$	3508	3491	-17
$7/2_1^+$	3778	3628	-150
$5/2_3^+$	3971	4048	77
$7/2_1^-$	4471	4227	-244
$5/2_4^+$	5012	5055	43
$3/2_4^+$	5075	4856	-219
$5/2_1^-$	5167	5190	23
$9/2_1^+$	5471	5503	32
$5/2_2^-$	5560	**5416**	-144

TABLE III – *Continued from previous page*

J_i^π	PSDPF (keV)	Exp (keV)	ΔE (keV)
$7/2_2^-$	5639	**5406**	-233
$9/2_1^-$	5696	5453	-243
$11/2_1^-$	5813	5639	-174
$7/2_2^+$	5912	**5729**	-183
$5/2_3^-$	5915	**5810**	-105
$7/2_3^-$	5991	**5926**	-65
$7/2_4^-$	6135	**5991**	-144
$7/2_3^+$	6210	**6325**	115
$3/2_5^+$	6364	**6502**	138
$9/2_2^+$	6510	**6424**	-86
$5/2_5^+$	6536	**6625**	89
$7/2_4^+$	6554	**6555**	1
$9/2_4^-$	6722	6810	88
$11/2_2^-$	6976	6987	11
$13/2_1^-$	7222	6936	-286
$11/2_4^-$	7850	**7998**	148
$13/2_2^-$	7991	**8086**	95
$15/2_1^-$	9094	9078	-16

TABLE IV: Possible correspondences between states calculated in the shell model for ^{34}P using the PSDPF interaction and the observed states. The calculation comprises both 0p-0h (positive-parity) and 1p-1h (negative-parity) states. The newly observed experimental states are shown in boldface (normal text). The last column expresses the energy difference between experimental and estimated states (ΔE).

J_i^π	PSDPF (keV)	Exp (keV)	ΔE (keV)
2_1^+	383	429	46
1_2^+	1479	1608	129
2_1^-	2182	2229	47
4_1^-	2196	2305	109
3_1^-	2354	2321	-33
5_1^-	3329	3352	23
3_2^-	3724	3752	28
5_2^-	3936	3951	15
4_3^-	3972	3911	-61
1_4^+	4054	**3806**	-248
2_4^+	4206	**4424**	218
4_4^-	4388	4455	67
3_2^+	4526	**4729**	203
2_7^-	4588	**4571**	-17
3_6^-	4684	**4613**	-71
6_1^-	4775	4630	-145
5_3^-	4811	**4710**	-101
2_8^-	5033	5013	-20
5_4^-	5219	**5344**	115
6_2^-	5422	5394	-28
5_5^-	5469	**5594**	125

TABLE IV – *Continued from previous page*

J_i^π	PSDPF (keV)	Exp (keV)	ΔE (keV)
6_3^-	5710	5726	16
5_6^-	5836	**5788**	-48
4_{11}^-	5993	**5975**	-18
4_{12}^-	6143	**6118**	-25
4_{13}^-	6272	**6174**	-98
5_7^-	6301	6193	-108
7_1^-	6371	6357	-14
5_8^-	6415	**6317**	-98
4_{14}^-	6545	**6445**	-100
6_4^-	6623	**6295**	-328
6_5^-	6779	**6923**	144
7_2^-	6951	**6991**	40
5_{10}^-	7050	**7066**	16
7_3^-	7256	**7256**	0
6_7^-	7444	7426	22
6_8^-	7614	**7590**	-24
7_4^-	7769	7919	150

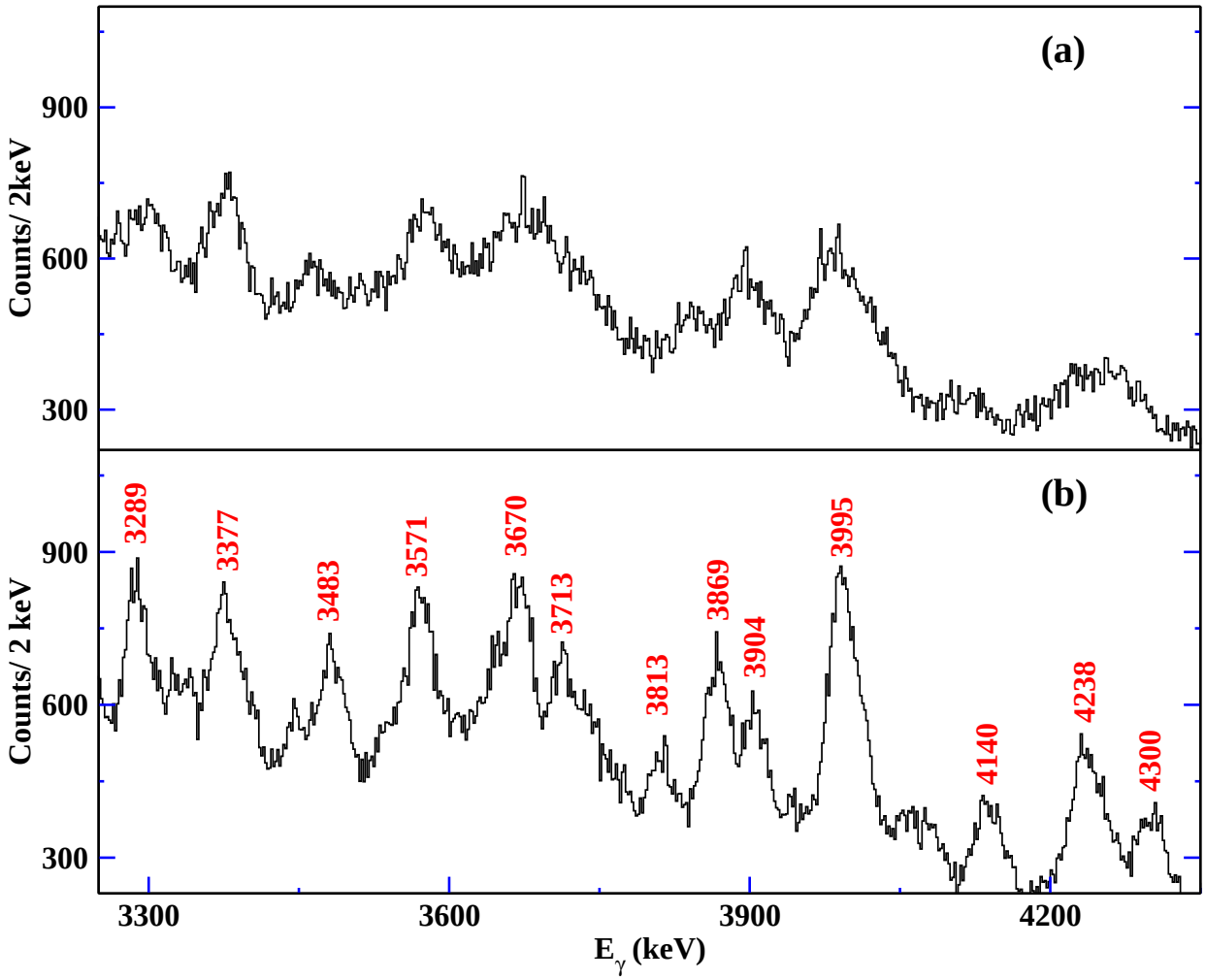

FIG. 1. Comparison between portions of two spectra in coincidence with protons and 429-keV γ rays in ^{34}P illustrating the power of kinematic reconstruction in improving the resolution; (a) and (b) Doppler corrected spectrum before and after kinematic reconstruction, respectively.

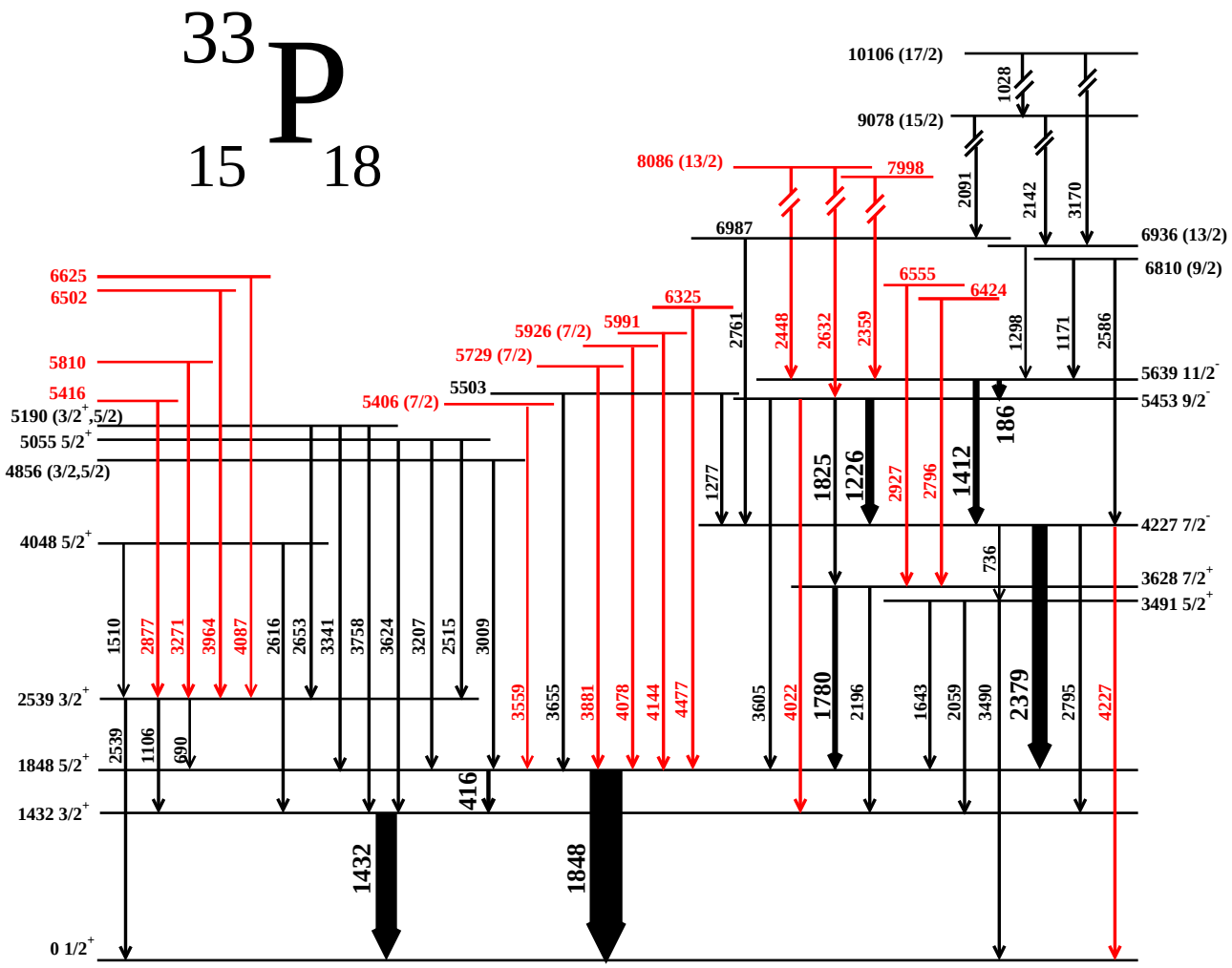

FIG. 2. The level scheme of ^{33}P established from the current analysis. States and transitions in red (gray) have been observed for the first time. The spins in the figure are from the current analysis and also from the literature. The arrow widths are proportional to the relative intensities of the γ-ray transitions. Those with less than 5% intensity are drawn with the same width.

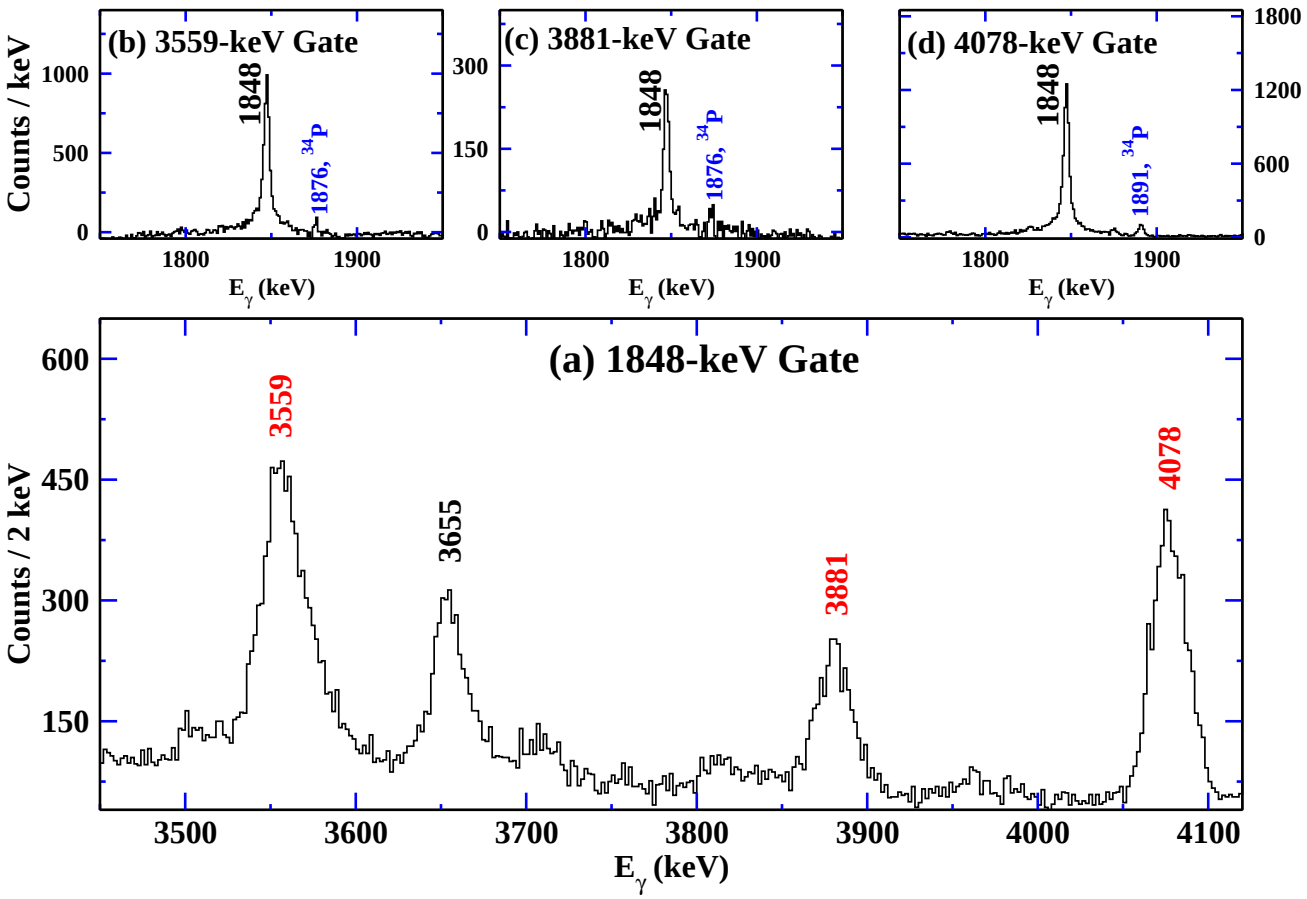

FIG. 3. Coincident spectra showing some γ transitions in ^{33}P . (a) 1848 gate, the newly observed γ peaks are labeled in red (gray) whereas the previously observed ones are labeled in black. (b) 3559 keV, (c) 3881 keV , and (d) 4078 keV gates, showing the reverse coincidence. The very strong ^{34}P line appears weakly in the broad high energy ^{33}P gates because of overlaps from broad lines in ^{34}P. ^{33}P and ^{34}P result from pn and 2pn evaporation and are not separated by the proton detection.

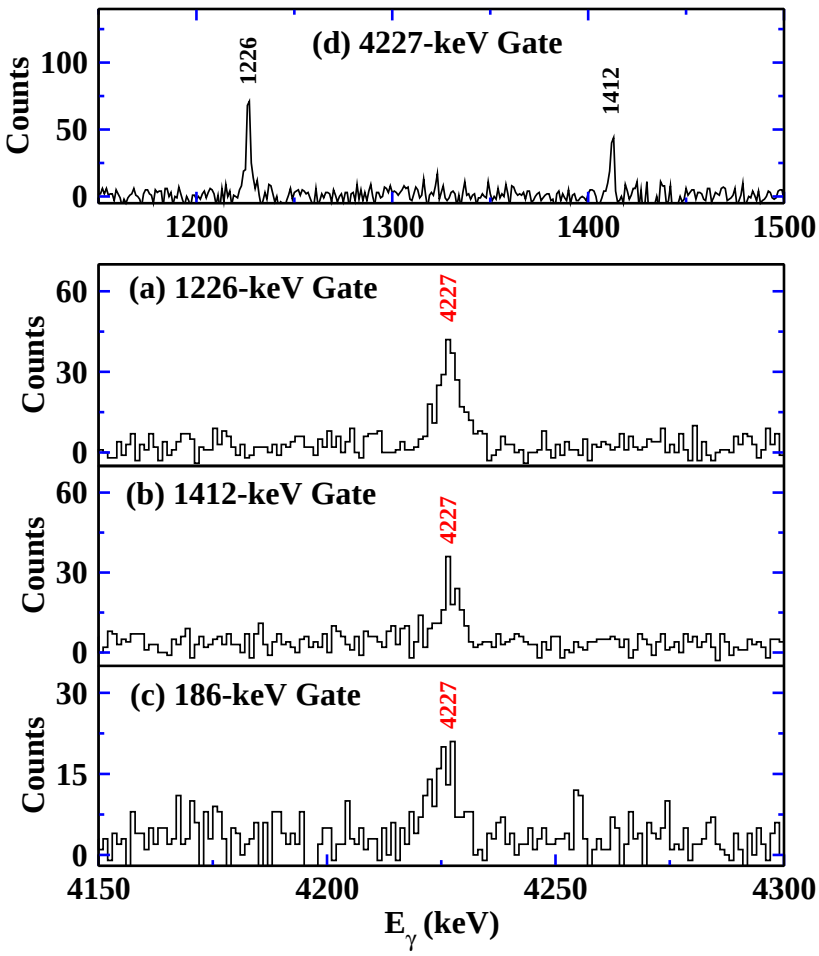

FIG. 4. Coincidence spectra confirming the placement of the 4227-keV transition in ^{33}P; (Top) the gate is on the 4227-keV γ ray itself, (a-c) gates on three transitions in coincidence with the 4227-keV line. Note the change in energy scale between the top spectrum and the three others.

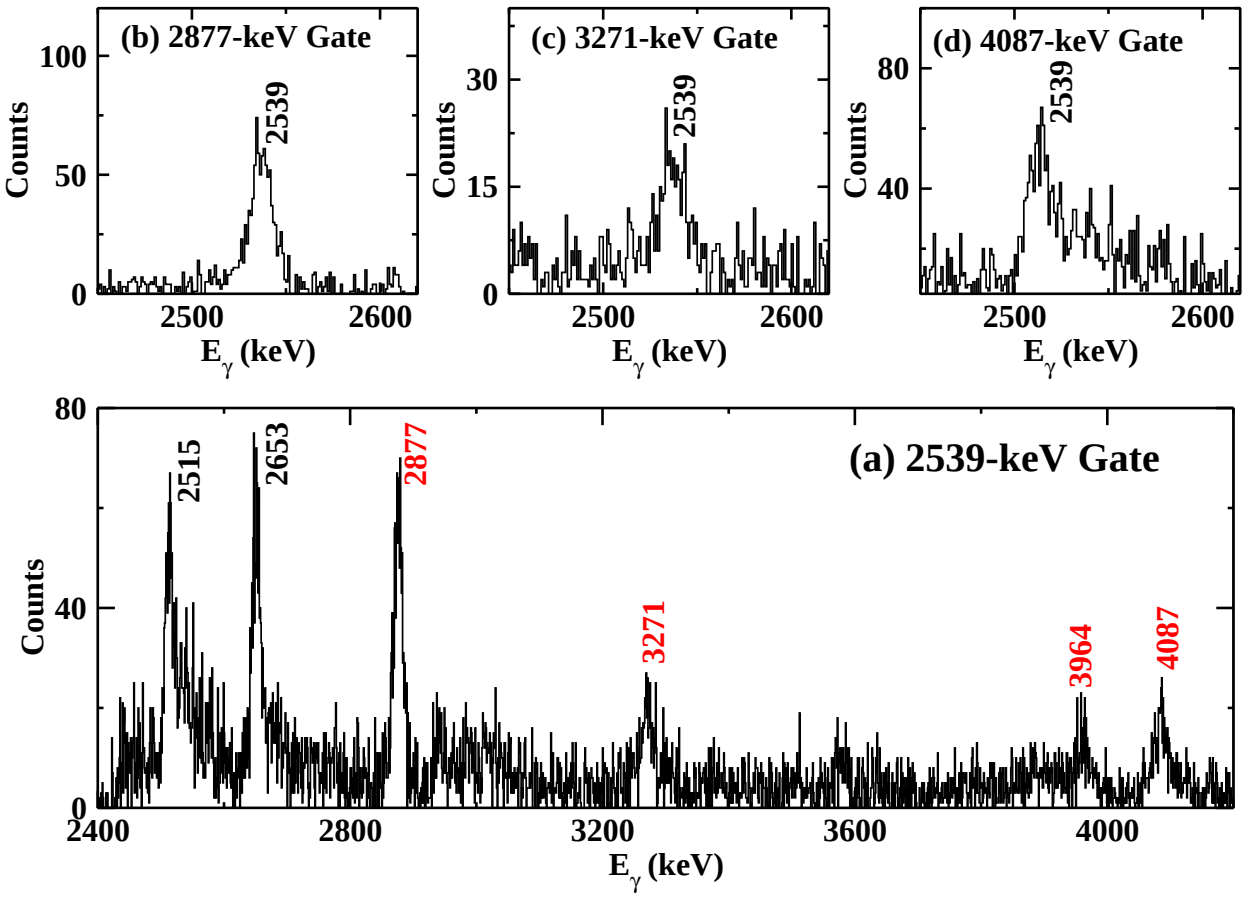

FIG. 5. Coincident spectra showing some transitions in (a) the 2539-keV gate in the Doppler-corrected matrix of ^{33}P. The newly observed γ lines are labeled in red, whereas the previously observed ones are labeled in black; (b) 2877-keV, (c) 3271-keV, and (d) 4087-keV gates, showing the reverse coincidence relationships.

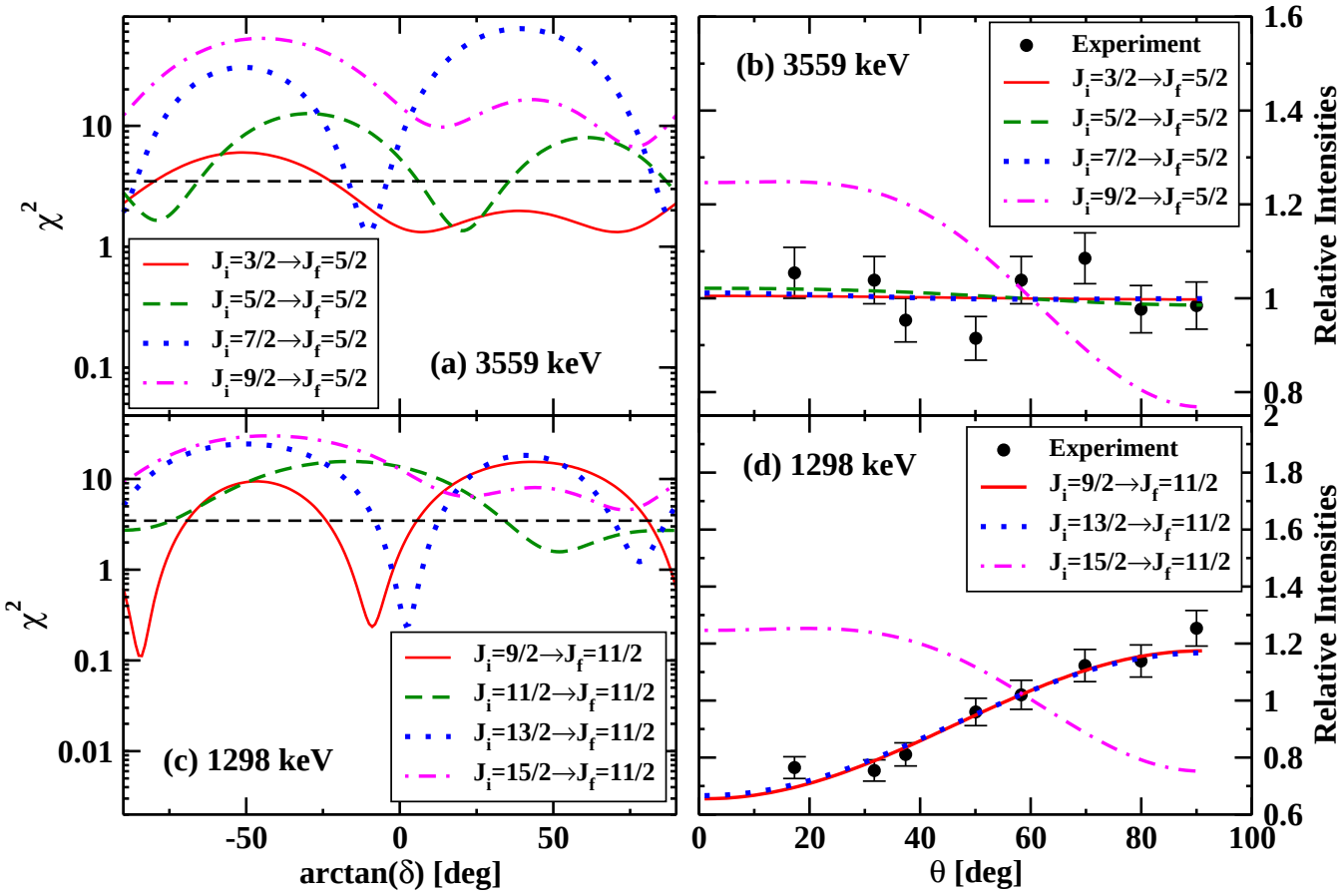

FIG. 6. (a), (c) χ^2 fits to the measured angular distribution for different spin hypotheses are plotted as function of mixing ratio, δ, for γ transitions in ^{33}P indicated in the panels. (b), (d) Angular distributions of 3559 and 1298-keV transitions for different spin hypotheses.

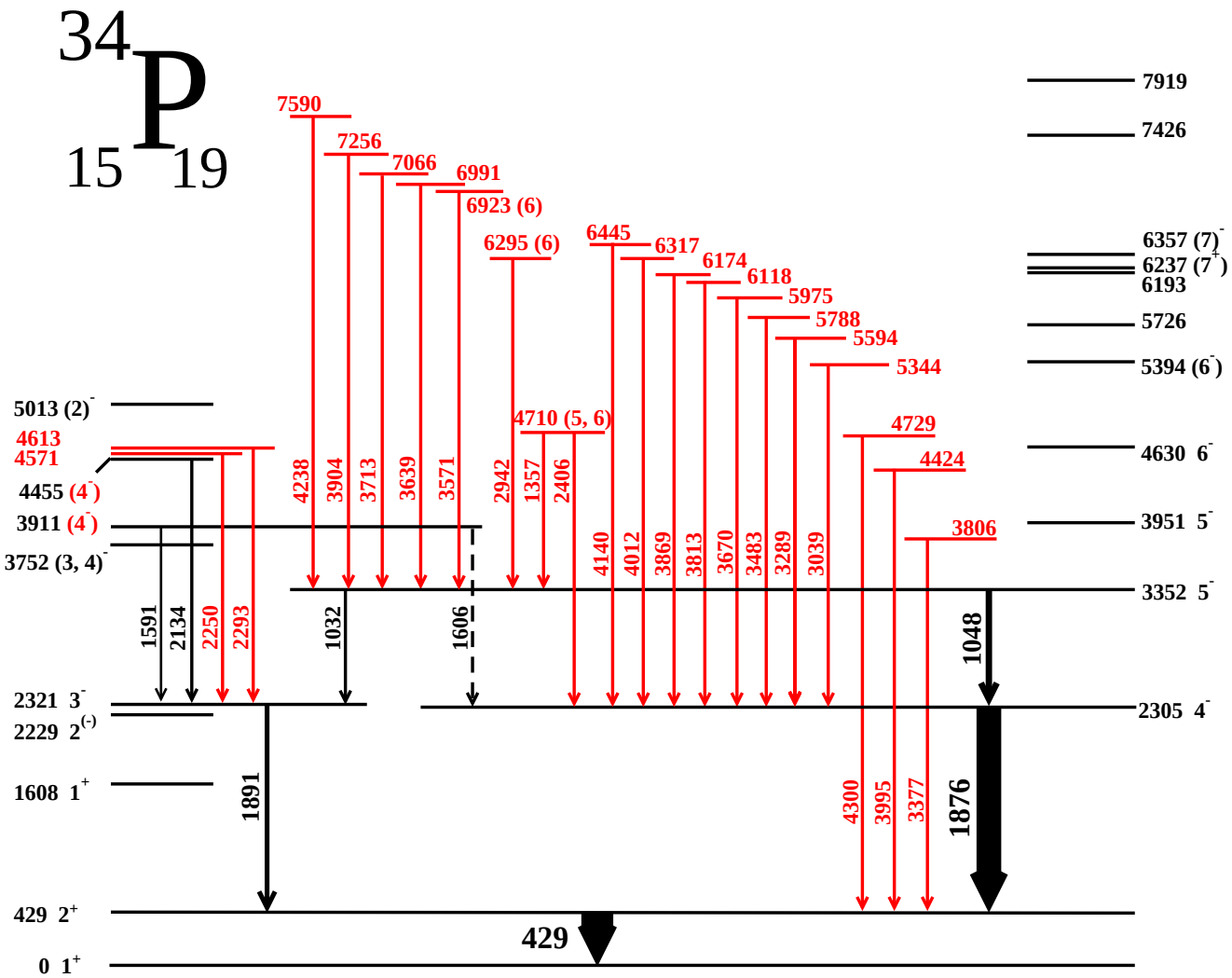

FIG. 7. The proposed, updated, level scheme of ^{34}P constructed from the present analysis. The newly observed states and transitions are marked in red (gray). The spins in the figure are from the current analysis and also from the literature. The arrow widths are proportional to the γ emission relative intensities. The transitions that were observed in the earlier analysis (see figure 1 in Ref. [21]) from the same data set, but not in coincidence with the newly observed transitions, are also verified, but not shown here for simplicity. Transitions with less than 5% intensity are drawn with the same width.

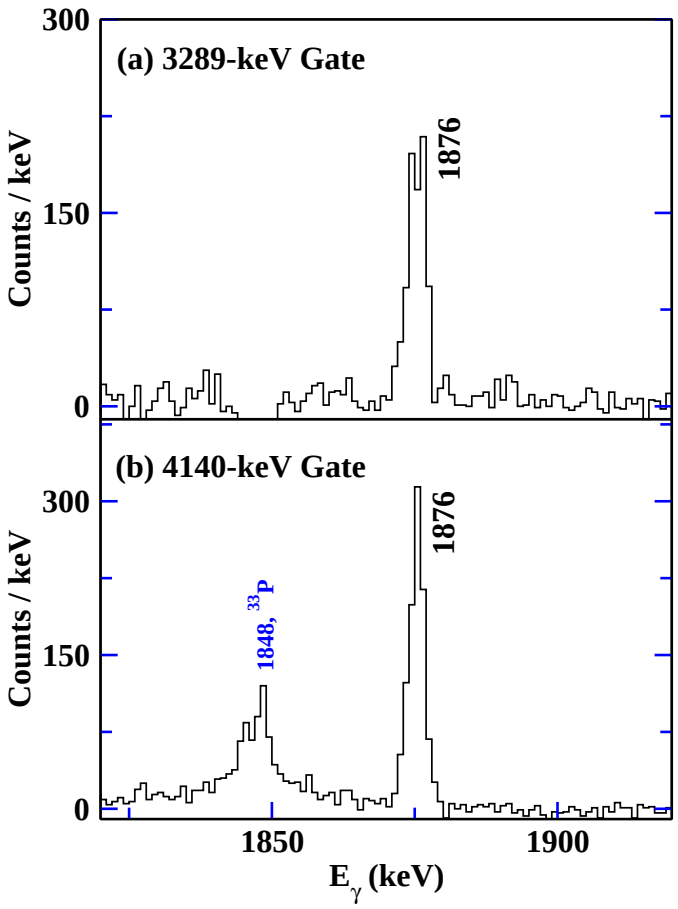

FIG. 8. Confirmation of the coincidence relationship of some newly assigned γ rays in ^{34}P, observed in the 429-keV gate projected on the Doppler-corrected axis in figure 1(b). One of the strongest ^{33}P lines appears weakly in panel (b), because of the overlap of 4144-keV line in ^{33}P with the 4140-keV one.

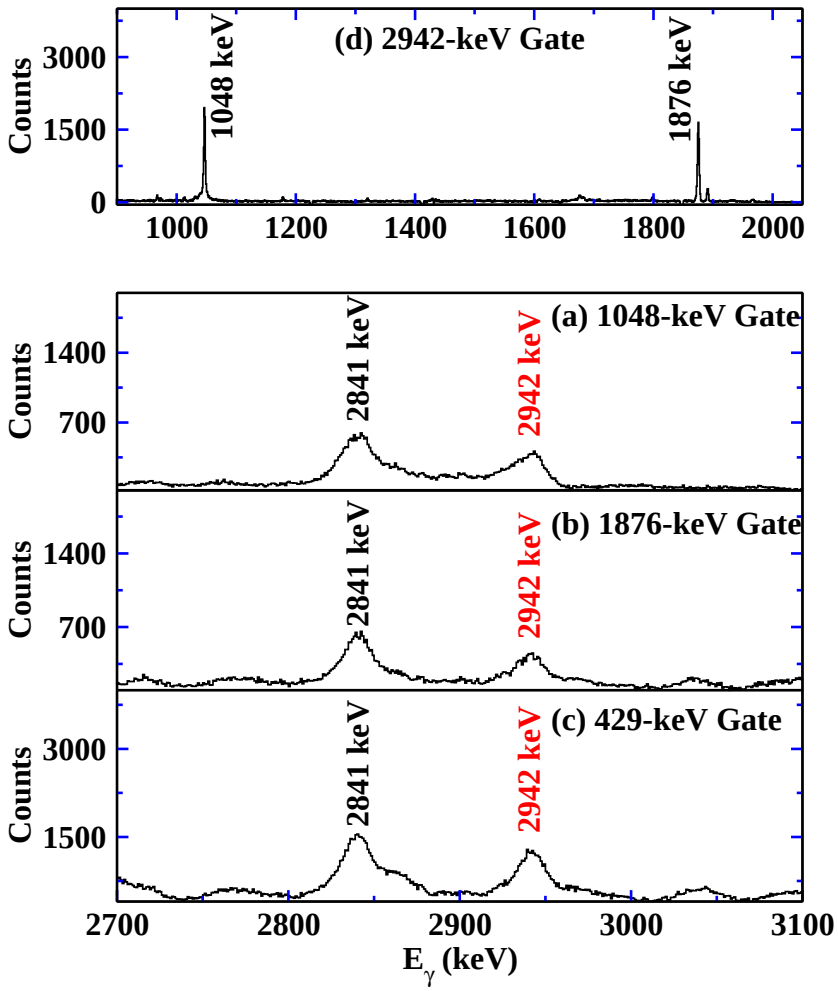

FIG. 9. (a) 1048-, (b) 1876-, and (c) 429-keV gates showing the new position of the 2942-keV transition in ^{34}P. (d) 2942-keV gate illustrating the consistency in coincidence relations.

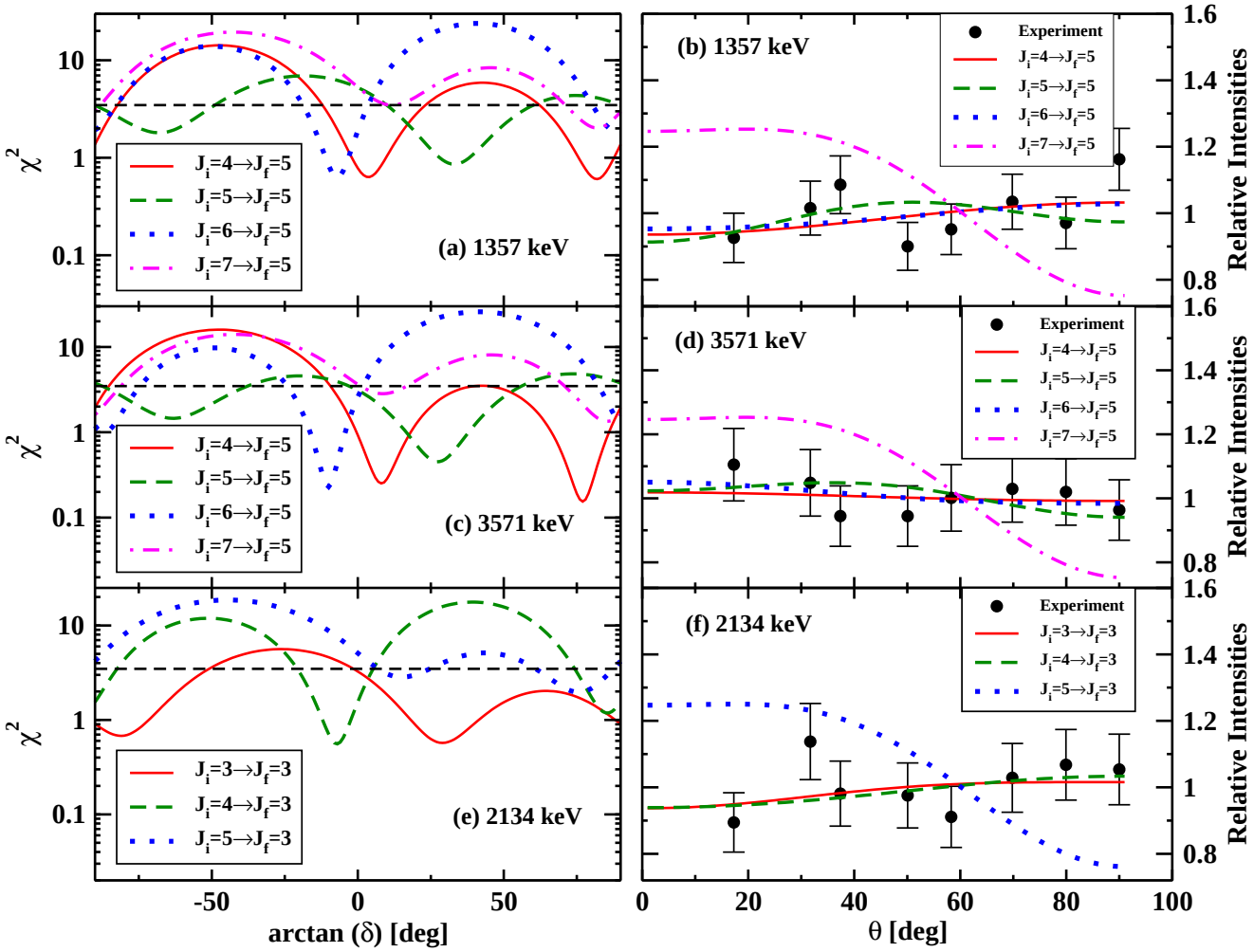

FIG. 10. χ^2 fits to the measured angular distribution for different spin hypotheses are plotted as a function of mixing ratio δ for selected transitions in ^{34}P indicated in the panels. The corresponding angular distributions for different spin hypotheses are plotted alongside.

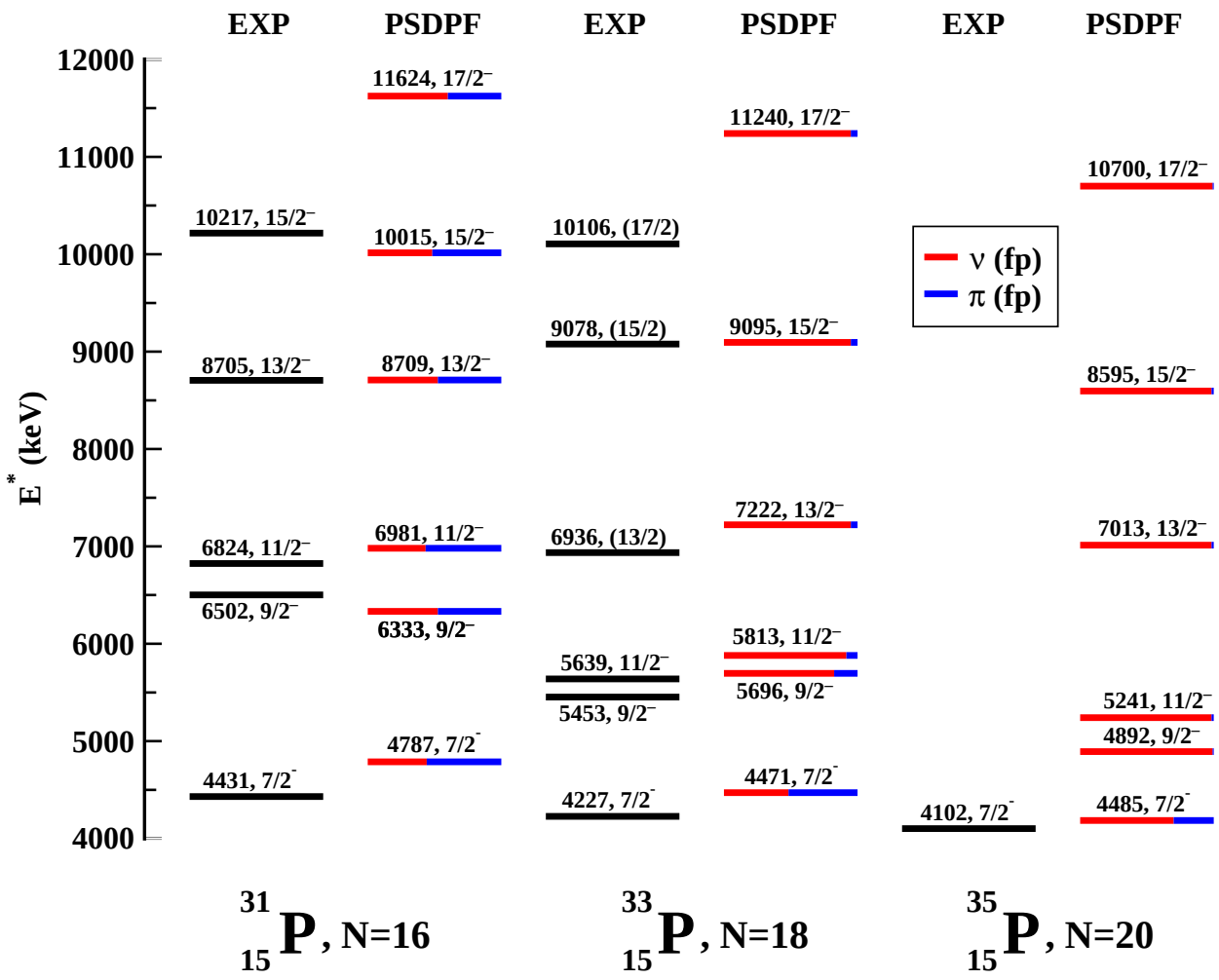

FIG. 11. Experimental negative-parity yrast states and their shell-model counter parts calculated with the PSDPF interaction along with the fp shell occupancy in the odd-mass phosphorus isotopes, ^{31}P, ^{33}P and ^{35}P. The red (light gray) and blue (dark gray) colors represent neutron and proton fp shell occupancies, respectively.

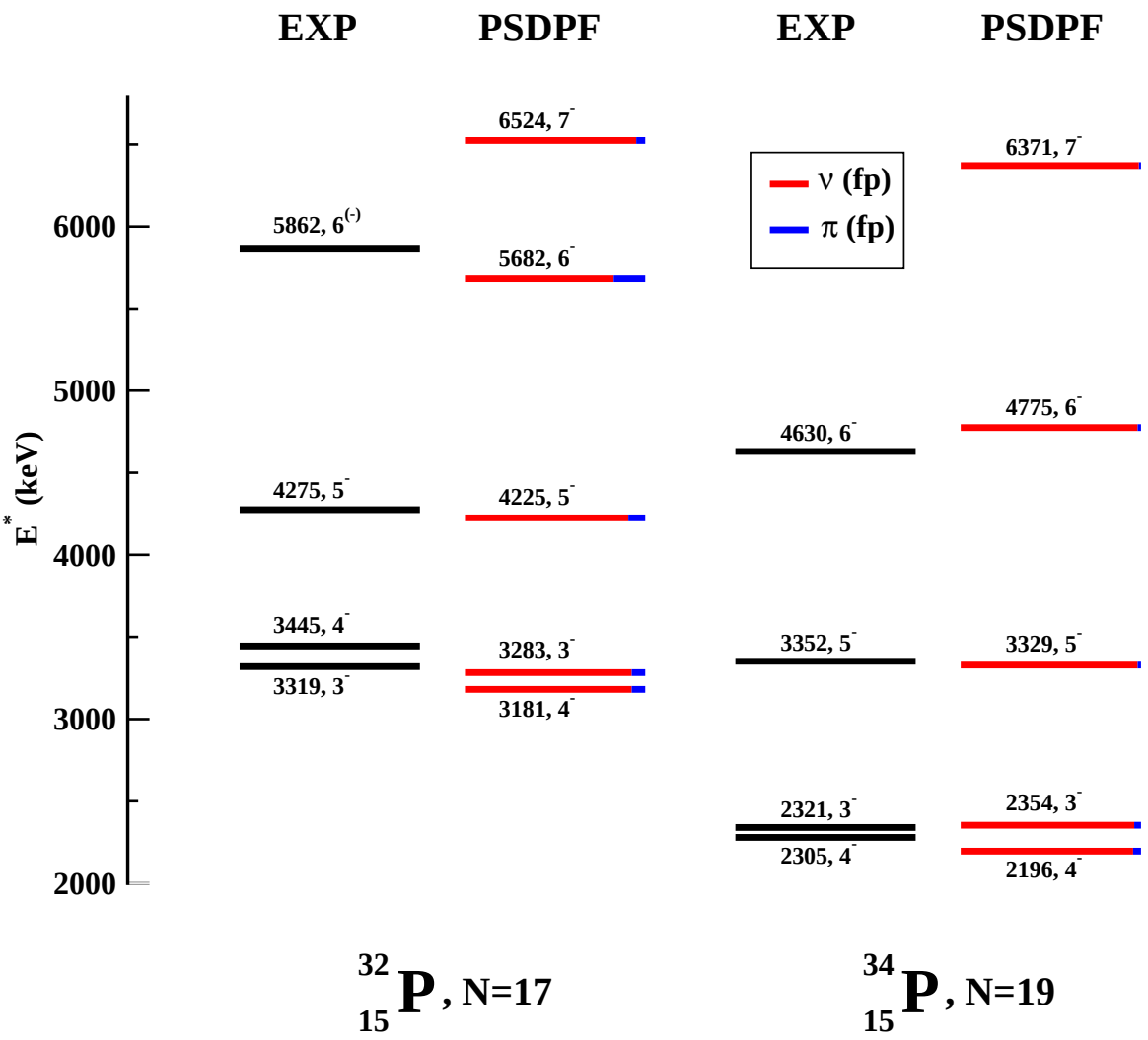

FIG. 12. Experimental negative-parity yrast states and their shell-model counter parts calculated with the PSDPF interaction along with the fp shell occupancy in the even-mass phosphorus isotopes, ^{32}P and ^{34}P. The red (light gray) and blue (dark gray) colors represent neutron and proton fp shell occupancies, respectively.